Nat. Hazards Earth Syst. Sci. Discuss., 2, 3499–3531, 2014
www.nat-hazards-earth-syst-sci-discuss.net/2/3499/2014/
doi:10.5194/nhessd-2-3499-2014

Natural Hazards and Earth System Sciences
Open Access
Discussions

Resolving vorticity-driven lateral fire spread using the WRF-Fire coupled atmosphere-fire numerical model

C. C. Simpson[1], **J. J. Sharples**[1], **and J. P. Evans**[2]

[1]Applied and Industrial Mathematics Research Group, School of Physical, Environmental and Mathematical Sciences, University of New South Wales, Australia
[2]Climate Change Research Centre, Faculty of Science, University of New South Wales, Australia

Received: 21 March 2014 – Accepted: 27 March 2014 – Published: 16 May 2014

Correspondence to: C. C. Simpson (c.simpson@adfa.edu.au)

Published by Copernicus Publications on behalf of the European Geosciences Union.

Abstract

Fire channelling is a form of dynamic fire behaviour, during which a wildland fire spreads rapidly across a steep lee-facing slope in a direction transverse to the background winds, and is often accompanied by a downwind extension of the active flaming region and extreme pyro-convection. Recent work using the WRF-Fire coupled atmosphere-fire model has demonstrated that fire channelling can be characterised as vorticity-driven lateral fire spread (VDLS). In this study, 16 simulations are conducted using WRF-Fire to examine the sensitivity of resolving VDLS to spatial resolution and atmosphere-fire coupling within the WRF-Fire model framework. The horizontal grid spacing is varied between 25 and 90 m, and the two-way atmosphere-fire coupling is either enabled or disabled. At high spatial resolution, the atmosphere-fire coupling increases the peak uphill and lateral spread rate by a factor of up to 2.7 and 9.5. The enhancement of the uphill and lateral spread rate diminishes at coarser spatial resolution, and VDLS is not modelled for a horizontal grid spacing of 90 m. The laterally spreading fire fronts become the dominant contributors of the extreme pyro-convection. The resolved fire-induced vortices responsible for driving the lateral spread in the coupled simulations have non-zero vorticity along each unit vector direction, and develop due to an interaction between the background winds and vertical return circulations generated at the flank of the fire front as part of the pyro-convective updraft. The results presented in this study demonstrate that both high spatial resolution and two-way atmosphere-fire coupling are required to reproduce VDLS within the current WRF-Fire model framework.

1 Introduction

The dynamic escalation of wildland fires into large conflagrations represents a major challenge to the management of fires in the landscape. Multi-scale interactions between a fire and the local fire environment, namely the topography, fuel and weather

NHESSD

2, 3499–3531, 2014

(Countryman, 1971), can produce complex fire behaviour that can cause a fire to rapidly grow in size, and potentially escape containment measures. Dynamic fire behaviour can not currently be predicted accurately using operational fire spread models, which typically treat fire behaviour in a quasi-steady state manner (Sullivan, 2009a, b, c). Understanding the physical processes that underpin these complex modes of fire propagation is therefore a key step towards improving the planning, preparedness, response and recovery surrounding the incidence of extreme fires.

A number of dynamic modes of fire propagation have been identified that do not fit a quasi-steady state description. For example, Viegas (2005) and Dold and Zinoviev (2009) examined the ability of a fire to exhibit exponentially increasing rates of spread up steep slopes and canyons, while Viegas et al. (2012) and Sharples et al. (2013b) discussed the abrupt increases in rate of spread that can occur when two lines of fires intersect at some oblique angle. Clark et al. (1996a, b) used an early version of the CAWFE coupled atmosphere-fire model to examine dynamic fingering, in which rotating columns of air near the fire front can drive rapid fire spread ahead of the main fire front. Another form of dynamic fire propagation, which was shown to be an important driver of extreme fire development in the 2003 Canberra bushfires (McRae, 2004; Sharples et al., 2012) and possibly also the 2009 Victorian bushfires (Price and Sharples, 2013), involves the rapid lateral propagation of a fire across a steep lee-facing slope in a direction approximately perpendicular to the prevailing wind direction. Originally referred to as "lee-slope channelling" and then "fire channelling", due to a supposed channelling of the winds under action of the fire and terrain, this phenomenon has subsequently been investigated using small-scale laboratory experiments (Sharples et al., 2010; Farinha, 2011) and a two-way coupled atmosphere-fire model known as WRF-Fire (Mandel et al., 2011; Coen et al., 2013) by Simpson et al. (2013) and Sharples et al. (2013a).

Simpson et al. (2013) used WRF-Fire to conduct a series of idealised simulations to model the evolution of a wildland fire burning on the lee-facing slope of a triangular ridge oriented perpendicular to the prevailing winds. Their study concluded that the

NHESSD
2, 3499–3531, 2014

lateral fire spread is vorticity-driven, and that the vorticity is generated through an interaction between topographically modified winds and the pyro-convection associated with the modelled fire. This permits fire channelling to be characterised as vorticity-driven lateral spread (VDLS), which it will be referred to as throughout the remainder of this study. Sharples et al. (2013a) extended the study by Simpson et al. (2013) to consider the effect of the prevailing wind speed on VDLS, and discovered a threshold wind speed of approximately $5\,m\,s^{-1}$ for the occurrence of VDLS under a fixed set of fuel properties and topography. The VDLS research to date has demonstrated that VDLS can result in rapid variations in fire behaviour with little change in the ambient fire environment conditions, thus posing a serious risk to civilians and fire fighters. However, the sensitivity of the VDLS characteristics to the surrounding environmental conditions is still not well understood.

WRF-Fire is one of a small number of coupled atmosphere-fire models that are capable of directly modelling the two-way coupled feedbacks between wildland fire behaviour and the atmosphere. Other examples include the HIGRAD/FIRETEC coupled atmospheric transport/wildland fire behaviour model developed at Los Alamos National Laboratory (Linn et al., 2002, 2007; Cunningham and Linn, 2007; Pimont et al., 2012), and MesoNH-ForeFire (Filippi et al., 2009, 2011), which couples a non-hydrostatic meso-scale model (Lafore et al., 1998) with a physical fire spread model described by Balbi et al. (2007). The development and use of these coupled models is critical for investigating the nature of dynamic fire-atmosphere interactions, which can be used to improve the simpler empirically-based models used to support operational fire management.

This study aims to examine the sensitivity of VDLS characteristics, in particular the average and peak lateral spread rate, to both the spatial resolution and atmosphere-fire coupling in the WRF-Fire model. It is expected that the occurrence of VDLS in WRF-Fire is dependent on resolving the fire-induced atmospheric dynamics responsible for driving the lateral fire spread across a steep lee-facing slope. We therefore expect to find a threshold horizontal and vertical grid spacing in WRF-Fire for the occurrence of

NHESSD
2, 3499–3531, 2014

VDLS, which will provide some indication of the spatial and temporal scale at which the dynamical fire-terrain-wind interaction driving the lateral spread operates. The WRF-Fire model and the configuration adopted in this study is discussed below, followed by the simulation results and then conclusions.

2 Numerical modelling

2.1 WRF-Fire

The coupled atmosphere-fire numerical model used in this study is the version of WRF-Fire, also known as WRF-SFIRE (Mandel et al., 2011; Coen et al., 2013), that is available as part of version 3.5 of the Weather Research and Forecasting (WRF) numerical weather prediction (NWP) model (Skamarock et al., 2008). The WRF-Fire model evolved from the CAWFE model (Clark et al., 2004; Coen, 2005) and has been validated for wildland fires across varying spatial scales (Kochanski et al., 2013a, b, c, d). The model has also been used to investigate fire-atmosphere interactions in the 2007 Kangaroo Island bushfires in Australia (Peace and Mills, 2012). Simpson et al. (2013) and Sharples et al. (2013a) used an earlier version of WRF-Fire in their numerical investigation of VDLS, and a similar model configuration is adopted in this study.

WRF utilises fully compressible non-hydrostatic equations and a mass-based terrain-following coordinate system. In this study, WRF is used in a large eddy simulation configuration (WRF-LES) (Moeng et al., 2007; Mirocha et al., 2010; Kirkil et al., 2012). WRF-LES explicitly resolves the grid-scale atmospheric eddies, whereas the subgrid-scale motions are modelled using a subfilter-scale stress model. WRF-LES is well suited to studying micro-scale turbulent atmospheric flows, such as those associated with VDLS.

The WRF-Fire model combines WRF-LES with a two-dimensional surface wildland fire spread model, known as SFIRE (Mandel et al., 2011). In SFIRE, multiple wildland fires can be ignited, and each fire is modelled as a temporally evolving perimeter that

NHESSD
2, 3499–3531, 2014

advances through the model domain using a level set function. The SFIRE model grid is defined on a subgrid of the WRF-LES horizontal model grid, and the horizontal extent of the SFIRE and WRF-LES model domains coincide. The terrain in SFIRE is defined at a higher spatial resolution than in WRF-LES when the subgrid ratio is greater than 1, but is otherwise identical. A total of 13 different fuel types are available in SFIRE, which are based on the 13 Anderson fuel categories (Anderson, 1982). The parameterised properties unique to each fuel type include the initial mass loading, fuel depth, surface area to volume ratio, moisture content of extinction and rate of mass loss following ignition.

The fire spread rate is calculated each time step at each point along the fire perimeter using a modified version of Rothermel's fire spread rate equation (Rothermel, 1972; Mandel et al., 2011):

$$R = R_0(1 + \phi_W + \phi_S) \quad (1)$$

where R is the rate of spread, R_0 is the base rate of spread in the absence of wind or slope, ϕ_W is the wind correction factor and ϕ_S is the slope correction factor. R_0 is calculated based upon the local parameterised fuel properties, ϕ_S is calculated using the local terrain slope, and ϕ_W is calculated using the wind speed and direction at the mid-flame height. The mid-flame height wind speed is calculated for each SFIRE model grid cell through the application of a fuel type dependent wind speed reduction factor to the horizontally and vertically interpolated WRF-LES winds at 6.1 m a.g.l.

Two-way atmosphere-fire coupling is achieved in WRF-Fire through the conversion of fuel mass to latent and sensible heat in SFIRE, which is injected each time step into WRF-LES and can subsequently affect the local atmospheric conditions, including the mid-flame height winds. WRF-Fire is therefore capable of directly modelling the interactions between a wildland fire, the atmosphere and terrain. For each kilogram of fuel combusted in SFIRE, 17.43 MJ of sensible heat is produced, and the sensible heat flux is inserted as an additional source term to the equation for the potential temperature in WRF-LES. The corresponding latent heat flux, which is inserted as a source term

NHESSD
2, 3499–3531, 2014

for the water vapour concentration, is fuel type dependent, and is around a factor of ten smaller than the sensible heat flux for the fuel type used in this study. The sensible and latent heat fluxes are individually aggregated across the SFIRE model subgrid and used to calculate the heat fluxes for each WRF-LES model grid vertical column. The vertical distribution of the heat fluxes within each WRF-LES model grid column is controlled by an exponential decay function, with the greatest quantity of sensible and latent heat injected into the lowest model vertical levels. The two-way coupling in WRF-Fire can be switched off by applying a multiplier of zero to the heat fluxes calculated by SFIRE.

2.2 WRF-Fire configuration

WRF-Fire is used in this study to conduct 16 simulations, which are divided into two groups of eight simulations with heat fluxes enabled and then disabled. Within each group, the WRF-LES horizontal and vertical grid spacing is set to 25, 30, 40, 50, 60, 70, 80 and 90 m. The subgrid ratio used between the SFIRE and WRF-LES model grids is set to eight in each simulation. This range of grid spacings was chosen as it sufficiently demonstrates the effect of spatial resolution on modelling VDLS with WRF-Fire. Individual simulations are named according to whether the atmosphere-fire coupling is enabled (C) or disabled (N), followed by the horizontal grid spacing in metres. For example, C30 is a coupled simulation with a horizontal grid spacing of 30 m, and N60 is a non-coupled simulation with a horizontal grid spacing of 60 m.

In this study, WRF-Fire is used in a highly idealised configuration, with many of the WRF physics schemes disabled, including the microphysics, longwave radiation, shortwave radiation, urban surface physics, planetary boundary layer and cumulus parameterisations. Diffusion in physical space is calculated using the velocity stress tensor and eddy viscosities are calculated using a 3-D prognostic 1.5-order turbulence closure scheme. A Rayleigh damping scheme (Klemp et al., 2008) is used in the top 1 km of the model to absorb upward propagating gravity wave energy and also dampens the pyro-convection in this layer. The lateral and top boundary conditions are open ra-

NHESSD
2, 3499–3531, 2014

diative, whereas the lower boundary is free-slip. The main model time integration in WRF-Fire is performed using a third-order Runge–Kutta scheme and the primary time step chosen is 0.0625 s. The secondary time step is a time-split small step for acoustic and gravity wave modes, and is set equal to one eighth of the primary time step. The initial 20 min of each simulation is considered the spin-up period and is not included in any of the time-averaging calculations. Only limited atmospheric turbulence is spun-up in WRF-Fire during the initialisation period, due to the absence of any sources of surface friction or surface heating prior to ignition of the fire in SFIRE. The total simulation time, including the spin-up period, is 2 h.

The horizontal extent of the WRF-Fire model domain is approximately 8 km × 8 km, and the number of WRF-LES and SFIRE model grid points varies with the horizontal and vertical grid spacing. A triangular-shaped ridge is located within both the WRF-LES and SFIRE model domains. The ridge's windward slope begins 2 km to the east of the western lateral boundary and the windward and leeward slope angles are 20° and 35° respectively. In contrast to the studies by Simpson et al. (2013) and Sharples et al. (2013a), the ridge's peak height is smaller, at around 600 m, and the ridge is tapered down at its southern and northern edges at an angle of 30°. A 400 m wide region of flat terrain is located at the southern and northern lateral boundaries to allow the background winds to flow smoothly around the ridge. A cubic spline interpolation is used to partially smooth the terrain edges, preventing any sharp edges in the terrain. The peak terrain height was reduced compared to previous studies in order to fit the isolated ridge within the model domain and keep an achievable computational run-time.

The WRF-Fire model top is initially set to 5 km and the vertical non-stretched grid spacing is initially equal to the horizontal grid spacing in WRF-LES. Due to use of sigma vertical levels there are minor variations in the vertical grid spacing with time, as the model top varies in height by up to 200 m in most simulations. Each simulation is initialised with horizontally homogeneous vertical profiles of the water vapour mixing ratio, potential temperature, and horizontal wind conditions. The water vapour mixing ratio is initially set to zero at all heights. The potential temperature is initially set to

NHESSD
2, 3499–3531, 2014

300 K between the surface and 4 km, and then increased linearly to 310 K between 4 and 5 km. This stable layer acts to prevent considerable descent of the model top towards the surface as the modelled pyro-convection affects the atmospheric pressure within the WRF-LES model domain. A temporally uniform westerly wind is prescribed at the western lateral boundary. The vertical wind profile at this boundary is given by $U(z)$ ($\mathrm{m\,s^{-1}}$):

$$U(z) = U_0 P(z) \hat{\boldsymbol{x}} \tag{2}$$

where U_0 denotes the reference wind speed, $P(z)$ prescribes the vertical wind profile and $\hat{\boldsymbol{x}}$ denotes the unit vector along the x-axis, towards the east. $P(z)$ is defined as:

$$P(z) = \begin{cases} \left(\frac{z}{200}\right)^{\frac{1}{7}}, & z \leq 200 \\ 1, & z > 200 \end{cases} \tag{3}$$

where z is the height in metres. In contrast to the studies by Simpson et al. (2013) and Sharples et al. (2013a), the wind profile power law has an exponent of 1/7. This exponent is a standard alternative to the logarithmic wind profile when the atmospheric stability is neutral (Justus et al., 1976). A logarithmic wind profile can not be used in this study due to the absence of a defined surface roughness. In this study, a background reference wind speed of $U_0 = 15\,\mathrm{m\,s^{-1}}$ is used.

Fuel type 13, which corresponds to the heavy logging slash Anderson fuel category (Anderson, 1982), is assigned homogeneously across the SFIRE model grid. Figure 1 shows the variation in time of the total heat flux for an SFIRE model grid cell following its ignition. The exponential decrease in the total heat flux is associated with a weighting parameter defined individually for each fuel type, and for the heavy logging slash fuel type results in a halving of the heat flux approximately every 15 min. For this fuel type, a wind reduction factor of 0.46 is applied to the WRF-LES horizontal winds at 6.1 m a.g.l. to determine the wind speed at the mid-flame height. This fuel type has a base rate of fire spread, in the absence of slope or wind, of around $0.14\,\mathrm{km\,h^{-1}}$. As

NHESSD
2, 3499–3531, 2014

the fuel type and slope are identical for each WRF-Fire simulation, any difference in the fire spread is due solely to variations in the mid-flame height wind conditions, and the subsequent dynamic atmosphere-fire coupling if the heat flux is enabled.

The modelled fire is ignited at the end of the 20 min spin-up period. The fire perimeter is ignited out to a distance of 40 m in all directions away from a south-north line of 200 m in length. This south-north line is centred on the y-axis and is located towards the base of the leeward slope, which emulates the laboratory experiments described by Sharples et al. (2010) and Farinha (2011). The fire is ignited symmetrically, starting from the northern and southern edges of the south-north ignition line and spreading towards the centre of the south-north line. Following this ignition process, the fire is allowed to spread freely throughout the model domain for the remainder of the simulation. The prescribed ignition is not included when calculating the spread rates presented below. In a real situation, a spot fire could be ignited in this location due to the transportation of firebrands downwind from a wildland fire located upwind of the leeward slope.

3 Results

3.1 Fire spread stages

The modelled wildland fire spread can be visualised using the ignition time for each SFIRE model grid cell and is shown for each WRF-Fire simulation in Fig. 2. Three distinct stages of fire spread can be identified from these simulations, not including the prescribed ignition described above:

1. Uphill: the fire front advances uphill from the ignition region to the ridge line.
2. Initial Lateral: the fire spreads laterally across the leeward slope at a rate much higher than the base rate of spread. This can occur during the uphill fire spread.

NHESSD
2, 3499–3531, 2014

3. Intermittent Lateral: the lateral extensions of the fire perimeter continue to spread intermittently, at a rate that is highest on the leeward slope and close to the ridge line.

In those coupled simulations with a horizontal grid spacing of 25 to 80 m, there is considerable lateral fire spread along the leeward slope, particularly near the ridge line. In contrast, there is no appreciable lateral fire spread subsequent to the prescribed ignition in the C90 and non-coupled simulations. This indicates that resolving the fine-scale fire-induced vorticity is critical for modelling VDLS with WRF-Fire.

3.2 Uphill fire spread in non-coupled simulations

In each non-coupled simulation, the initially flat fire front develops a parabolic shape as it advances uphill after the prescribed fire ignition. The parabolic shape develops as a consequence of the initial ignition shape and the method use in WRF-Fire to account for the effect of slope on the rate and direction of fire spread (Mandel et al., 2011). During the 25 to 30 min period following the prescribed ignition in which the fire advances uphill, the westerly spread rate typically varies between 1.0 and 1.2 $km\,h^{-1}$ for each simulation, as shown in Fig. 3a. This is approximately an order of magnitude larger than the base rate of spread in the absence of slope or wind. The limited variability in the westerly spread rate between the simulations indicates that resolution of the terrain-modified mid-flame height winds does not appreciably affect the uphill spread rate for this WRF-Fire model configuration. This result is not unexpected given the neutral atmospheric stability, strong winds across the ridge line, and low ridge line height of 600 m.

Once the fire front encounters the ridge line, the slope is no longer positive and the westerly spread rate decreases towards the base rate of spread. The fire continues to spread in all directions at approximately the base rate of spread for the remainder of the simulation, resulting in the slowly expanding fire perimeters seen in Fig. 2b. Figure 4 shows the time-averaged mid-flame height horizontal winds for the N25 simulation.

NHESSD
2, 3499–3531, 2014

The terrain-modified winds are fairly consistent in time after the WRF-Fire initialisation period and are weak across the leeward slope. The uphill fire spread rate is therefore dominated by the slope correction factor in the modified Rothermel equation.

3.3 Uphill and initial lateral fire spread in coupled simulations

The westerly spread rate is typically much more variable, both in time and between simulations, for the coupled simulations than for the non-coupled simulations, as demonstrated by directly comparing Fig. 3a and b. The peak 5 min averaged westerly spread rate is 2.90, 3.14, 2.28, 1.50 and 1.79 $\mathrm{km\,h^{-1}}$ in the C25, C30, C40, C50 and C70 simulations, compared with 1.16, 1.18, 1.20, 1.20 and 1.15 $\mathrm{km\,h^{-1}}$ in the N25, N30, N40, N50 and N70 simulations. This demonstrates that inclusion of the two-way coupled atmosphere-fire interactions in WRF-Fire can markedly affect the uphill spread rate and initial fire front development, particularly at higher spatial resolution. For the C60, C80 and C90 simulations, the peak 5 min averaged westerly spread rate is almost identical to the equivalent non-coupled simulations, indicating limited impact of the fire-modified atmospheric dynamics on the westerly spread rate.

In the coupled simulations, the fire front also initially develops a parabolic shape as it advances uphill from the prescribed fire ignition, similarly to in the non-coupled simulations. However, the turbulent fire-induced mid-flame height winds result in asymmetric fire front advancement, which represents the start of the initial lateral fire spread stage, prior to the fire front reaching the ridge line. The approximate time after ignition and height on the leeward slope of this initial lateral spread is provided in Table 1 for each coupled simulation, alongside the time at which the fire front first encounters the ridge line. The initial lateral fire spread typically begins earlier and lower on the leeward slope as the horizontal and vertical grid spacing decreases. This initial lateral spread prior to the fire front's arrival at the ridge line was not discussed by Simpson et al. (2013) and Sharples et al. (2013a), although both of those studies used a coarser WRF-Fire spatial resolution than that used in this study.

NHESSD
2, 3499–3531, 2014

In the C25 and C30 simulations, vortices with non-zero vertical and horizontal components are formed intermittently and non-symmetrically in close proximity to the fire perimeter during the uphill fire spread stage, as shown for the C25 simulation in Fig. 5. The vortices drive the initial lateral fire spread, to beyond the initial south-north extent prescribed in the ignition, during the uphill fire spread in both the C25 and C30 simulations. They also contribute towards the high peak 5 min averaged westerly spread rate of 2.90 and 3.14 $km\,h^{-1}$ in the C25 and C30 simulations. Vortices are also present during the uphill fire spread stage in the other coupled simulations, but they do not affect the uphill or lateral spread rate to the same extent as in the C25 and C30 simulations. These vortices are entirely absent in the non-coupled simulations, demonstrating that they form due to a combined interaction between the fire, terrain and wind.

In the C25, C30, C40, C50, C60 and C70 simulations, the fire advances at least several hundred metres beyond the ridge line, across the windward slope. In contrast, fire spread onto the windward slope was not recorded during fire channelling events in the 2003 Canberra bushfires (Sharples et al., 2012). The advancement of the modelled fire onto the windward slope can be partly attributed to the fire-induced easterly winds, which develop as an inflow towards the base of the pyro-convective updraft at the head of the fire front. These easterly winds can dominate over the background westerly winds across the leeward and upper windward slopes, and therefore facilitate fire spread across the upper windward slope. In addition, negative slopes are currently treated identically to a flat slope in WRF-Fire, so there is no reduction in the fire spread rate across a negative slope relative to a flat slope.

3.4 Intermittent lateral fire spread in coupled simulations

For those coupled simulations in which VDLS occurs, the lateral extensions of the fire front close to the ridge line become the most rapidly advancing parts of the fire perimeter once the uphill and initial lateral fire spread stages have concluded. The southerly and northerly fire fronts continue to advance laterally across the leeward slope in intermittent jumps for the remainder of the simulation, as demonstrated by Fig. 6a and

NHESSD
2, 3499–3531, 2014

b. The peak 5 min averaged lateral spread rate in the C25, C30, C40, C50, C60, C70, C80 and C90 simulations is a factor of 8.8, 9.6, 6.6, 13.3, 11.6, 5.9, 3.5 and 1.9 times higher than in the equivalent non-coupled simulations. The atmosphere-fire coupling is therefore shown to increase the lateral rate of spread, as further demonstrated by comparing the coupled and non-coupled lateral spread rates shown in Fig. 6.

The lateral fire spread occurs asymmetrically for each VDLS simulation, resulting in differences between the peak 5 min averaged southerly and northerly spread rate. Most commonly, the peak lateral spread rate is highest towards the north (C25, C30, C50, C70 and C80), rather than towards the south (C40 and C60), as shown in Fig. 6. Given the identical and symmetric terrain and prescribed ignition used in each coupled simulation, the asymmetry in the lateral fire spread must originate from numerical instability in the WRF-Fire model, caused by round-off error. The resulting asymmetries then grow in magnitude due to the effect of coupled atmosphere-fire feedbacks, and so are therefore associated with both the numerical instability within the WRF-Fire model, and the dynamical instability in VDLS. Similar asymmetric fire spread has been noted in the CAWFE model, which pre-dates WRF-Fire (Clark et al., 2004).

The occurrence and irregularity of the lateral fire spread across the leeward slope is attributable to the movement of fire-induced vortices across the flanks of the fire perimeter. The vortices typically form and dissipate on sub-minute time scales, and can only occasionally be tracked in the 1 min interval WRF-Fire model output. The three-dimensional vorticity vector field, $\boldsymbol{\omega}(x,y,z)$, is calculated in WRF-LES as the curl of the three-dimensional wind field, $\boldsymbol{v}(x,y,z)$. The characteristics of the vortices driving the initial lateral fire spread can be inferred for the C25 simulation from Figs. 5 and 7. They show that the vortices on the northern flanks of the fire are associated with clockwise rotation of the atmospheric flow about both the x-axis and z-axis. Although not shown, the vortices on the southern flanks are associated with counter-clockwise rotation about the x-axis and z-axis. The circulating flow at the mid-flame height driving the lateral fire spread is centred on the pyro-convectively driven vertical circulation, seen as adjacent updrafts and downdrafts close to the flanks of the fire perimeter

NHESSD
2, 3499–3531, 2014

in Fig. 5. The vertical circulations vary in size, location and intensity throughout the simulation as the fire front develops, but are frequently formed close to the lateral flanks of the fire front, such as at 28 and 32 min in the C25 simulation.

The horizontal and vertical grid spacing used in the WRF-Fire model affects the resolution of the fire-induced vortices, and therefore also the fire-atmosphere coupling and resulting lateral spread rates. For example, the average lateral spread rate after ignition is 0.88 and 1.04 $km\,h^{-1}$ in the C25 and C30 simulations, compared with lower values of 0.78, 0.71, 0.61, 0.42, 0.22 and 0.13 $km\,h^{-1}$ in the C40, C50, C60, C70, C80 and C90 simulations. It is possible that using even finer grid spacing in WRF-Fire could further increase the average and peak lateral spread rate. However, the similarity in the peak and average lateral spread rate between the C25 and C30 simulations suggests that a near-optimal resolution has been reached. In addition, it is difficult to complete a WRF-Fire simulation at higher resolution for an otherwise identical model configuration, due to the intense atmospheric turbulence associated with the fire.

3.5 Power and pyro-convection

The time at which the initial lateral fire spread begins in each VDLS simulation, presented in Table 1, manifests itself as a sudden increase in the domain-aggregated total heat release rate relative to the C90 simulation, as shown in Fig. 8. This occurs due to the ignition of areas of fuel along the leeward slope that would not have been ignited without VDLS, and is therefore a direct consequence of the enhanced rate of lateral and uphill fire spread relative to the equivalent non-coupled simulations. The peak 5 min averaged westerly spread rates in the C25 C30, C40, C50 and C70 simulations, which are relatively higher than the equivalent non-coupled simulations, occur in conjunction with the initial lateral fire spread, and are therefore also associated with the first sudden increase in the domain-aggregated total heat flux. This occurs at around 4, 5, 17, 27 and 20 min after ignition for the C25, C30, C40, C50 and C70 simulations.

Throughout the remainder of the simulation, the total heat release rate is considerably higher in the high-resolution coupled simulations than in the relatively low-

NHESSD
2, 3499–3531, 2014

resolution C90 simulation. The peak total heat release rate increases as the horizontal and vertical grid spacing decreases, and is around a factor of seven times greater in the C25 simulation than in the C90 simulation, as seen in Fig. 8. These results support the concept that VDLS is accompanied by intense pyro-convection, as discussed by (Sharples et al., 2012), due to the ignition of fuel along the leeward slope that provides an additional source of latent and sensible heat. The laterally spreading fire fronts become the dominant contributor to the total heat release rate after the fire front encounters the ridge line and the uphill fire stage concludes.

The release of sensible and latent heat from the modelled wildland fire into the surrounding atmosphere in the coupled simulations is of a sufficient magnitude for the near-fire and downwind atmospheric dynamics and turbulence to be dominated by pyro-convection. As the background flow is mostly laminar, particularly over 200 m away from the surface, it is possible to determine the resolved fire-induced mean kinetic energy of the turbulent portion of the atmospheric flow after ignition. Figure 9a shows the resolved turbulent kinetic energy (TKE), calculated for each WRF-LES model grid cell using time-averaging from ignition to the end of the simulation, for the C25 simulation. The TKE is clearly of a high magnitude downwind of the ridge line in the C25 simulation, due predominantly to the effects of pyro-convection rather than the terrain-induced turbulence. For comparison, the peak TKE in the WRF-LES model grid cells for the C25 and N25 simulations is 196.0 and 6.6 $m^2 s^{-2}$.

Simpson et al. (2013) and Sharples et al. (2013a) have previously demonstrated that the background winds over the ridge can tilt the fire plume relative to the ground. Tilting of the fire plume, intense pyro-convection, and a highly turbulent near-fire and downwind atmosphere provide favourable conditions for the downwind transport of embers or firebrands. This supports the hypothesis that extensive spotting of embers, or firebrands, is chiefly responsible for the downwind extension of the active flaming zone seen in real VDLS events, such as those in the 2003 Canberra bushfires (Sharples et al., 2012). However, WRF-Fire does not currently model long-range spotting directly,

NHESSD
2, 3499–3531, 2014

so therefore cannot be used to explicitly test the impact of long-range spotting during VDLS.

The sensible and latent heat released from the fire also directly affects the near-fire and downwind atmospheric potential temperature, and the time-averaged potential temperature is shown for the C25 simulation in Fig. 9b. Relative to the background potential temperature of 300 K up to a height of 4 km, the time-averaged potential temperature peaks at 319.0 K directly above the ridge line in the C25 simulation. Potential temperature anomalies greater than 1 K extend downwind from the fire, but without impinging on the surface downwind of the leeward slope. The pyro-convection in this situation is therefore not likely to contribute towards fuel pre-drying downwind of the ridge, as the warmer air above the fire is sufficiently buoyant to rise away from the surface in an atmosphere that initially has neutral stability. The potential temperature anomalies are more spatially confined than the fire-induced turbulence, so do not act as a good proxy measure of the extent of the pyro-convective plume.

4 Conclusions

The WRF-Fire simulations presented in this study clearly demonstrate that both high spatial resolution and two-way atmosphere-fire coupling are required for WRF-Fire to model VDLS on a steep lee-facing slope, which is consistent with the results presented by Simpson et al. (2013) and Sharples et al. (2013a). VDLS did not occur in the non-coupled simulations, regardless of spatial resolution, whereas VDLS occurred in most of the coupled simulations, aside from in the C90 simulation. The peak and average uphill and lateral fire spread rates in the coupled simulations typically decreased with spatial resolution, and the fire-atmosphere coupling enhanced the peak 5 min averaged uphill and lateral spread rate by a factor of 2.5 and 9.14 for the C25 simulation, and a factor of 2.7 and 9.50 for the C30 simulation. These results suggest that there is a size-limit for the fire-induced vortices that drive the lateral fire spread. Based on

NHESSD
2, 3499–3531, 2014

a minimum of 2 × 2 grid cells in WRF-LES to resolve an atmospheric eddy, the eddy diameter limit appears to be of the order of 160 to 180 m.

The fire fronts that develop and spread laterally across the steep lee-facing slope become the dominant contributor to the total heat release rate once the fire front reaches the ridge line. The laterally spreading fire fronts are therefore the dominant contributors of the intense pyro-convection, which results in a highly turbulent pyro-convective plume extending above the fire and downwind of the leeward slope. The tilting of the plume by the background winds, the intense pyro-convection, and the resulting highly turbulent near-fire and downwind atmospheric dynamics provide favourable conditions for spotting downwind of the fire. However, long-range spotting is not currently explicitly included in the WRF-Fire model.

The fire-induced vortices responsible for driving the lateral fire spread, and in some cases enhancing the uphill fire spread, can clearly be seen in the coupled high-resolution WRF-Fire simulations. The vortices have non-zero vorticity vector components along the $\hat{x}$, $\hat{y}$ and $\hat{z}$ unit vector directions, and form predominantly due to intense pyro-convection, rather than as a feature of the terrain-induced turbulence. The vortices are centred on pyro-convectively generated vertical circulations close to the modelled fire, and can drive the lateral fire spread when they cross over the lateral flank of the fire perimeter. It will be possible to better reconcile the vortex characteristics in VDLS with current knowledge of vorticity in wildland fires (Forthofer and Goodrick, 2011) using WRF-Fire model output at sub-minute intervals, which is planned in future work.

VDLS is an example of dynamic fire behaviour in complex terrain, and occurs due to an interaction between a wildland fire, the terrain, and the ambient winds. A number of environmental conditions need to be satisfied in order for VDLS to occur. For example, Sharples et al. (2013a) demonstrated that an ambient wind speed threshold, of around $5\,\mathrm{m\,s^{-1}}$, was required for VDLS to occur in an otherwise fixed set of fire environment conditions. The study by Sharples et al. (2012) indicated that VDLS was sensitive to the combined effects of terrain slope and aspect in the 2003 Canberra bushfires. However, this relationship has not yet been explored using numerical modelling or small-scale

NHESSD
2, 3499–3531, 2014

laboratory experiments. Further research is therefore needed to explore the sensitivity of VDLS to other aspects of the fire environment, in particular the fuel type, terrain slope and wind direction relative to the terrain. Additional sensitivity studies using the WRF-Fire model will improve our understanding of the parameter space in which VDLS occurs. It is expected that this will facilitate the development of a VDLS parameterisation in non-coupled fire spread models, and improve operational predictability of VDLS. The results presented in this study will ensure that the WRF-Fire model will be used at sufficiently high-resolution to capture VDLS in future work.

WRF-Fire is one of a small number of fire spread models currently capable of directly modelling the coupled interactions between a wildland fire and the atmosphere, and operates at a scale well suited for studying VDLS. However, the model has a number of limitations that need to be addressed in future work to facilitate an improved numerical investigation of VDLS. The semi-empirical fire spread model, based on Rothermel's fire spread rate equation (Rothermel, 1972), likely oversimplifies the dynamic interactions between the fire spread and atmosphere involved in real VDLS events. In addition, WRF-Fire does not currently have a spotting or crown fire model, such as those found in other fire spread models e.g. FARSITE (Finney, 1998). A spotting model will be implemented in future work to investigate the apparent role of spotting in the downwind extension of the active flaming region seen in VDLS events during the 2003 Canberra bushfires (Sharples et al., 2012).

Acknowledgements. This research was supported by the Australian Research Council through the Discovery Indigenous Award IN130100038, and was partially supported by the Australian Research Council as part of the Future Fellowship FT110100576. Additional support was provided through a UNSW Canberra Silver Star Award. The simulations and data analysis were conducted on the Raijin supercomputer, operated by the National Computational Infrastructure, using a computer grant supported by the Merit Allocation Scheme. We acknowledge Kevin Tory, Rick McRae, Jeff Kepert, Will Thurston and Robert Fawcett for useful discussions relating to this work.

NHESSD
2, 3499–3531, 2014

References

Anderson, H.: Aids to determining fuel models for estimating fire behaviour, Report, USDA Forest Service, Intermountain Forest and Range Experiment Station, 1982. 3504, 3507

Balbi, J., Rossi, J., Marcelli, T., and Santoni, P.: A 3-D physical real-time model of surface fires across fuel beds, Combust. Sci. Technol., 179, 2511–2537, 2007. 3502

Clark, T., Jenkins, M., Coen, J., and Packham, D.: A coupled atmosphere-fire model: convective feedback on fire-line dynamics, J. Appl. Meteorol., 35, 875–901, 1996a. 3501

Clark, T., Jenkins, M., Coen, J., and Packham, D.: A coupled atmosphere-fire model: role of the convective Froude number and dynamic fingering at the fireline, Int. J. Wildland Fire, 6, 177–190, 1996b. 3501

Clark, T., Coen, J., and Latham, D.: Description of a coupled atmosphere-fire model, Int. J. Wildland Fire, 13, 49–64, 2004. 3503, 3512

Coen, J.: Simulation of the Big Elk Fire using coupled atmosphere-fire modeling, Int. J. Wildland Fire, 14, 49–59, 2005. 3503

Coen, J., Cameron, M., Michalakes, J., Patton, E., Riggan, P., and Yedinak, K.: WRF-Fire: coupled weather-wildland fire modeling with the weather research and forecasting model, J. Appl. Meteorol. Clim., 52, 16–38, 2013. 3501, 3503

Countryman, C.: Fire Whirls. . . Why, When, and Where, Report, USDA Forest Service, Pacific Southwest Forest and Range Experiment Station, Berkeley, CA, 1971. 3501

Cunningham, P. and Linn, R.: Numerical simulations of grass fires using a coupled atmosphere-fire mode: dynamics of fire spread, J. Geophys. Res., 112, D05108, doi:10.1029/2006JD007638, 2007. 3502

Dold, J. and Zinoviev, A.: Fire eruption through intensity and spread interaction mediated by flow attachment, Combust. Theor. Model., 13, 763–793, 2009. 3501

Farinha, H.: Formação de Vórtices num Incêndio Florestal – Estudo Laboratorial de um Vórtice de Eixo Horizontal e de um Tornado de Fogo, Thesis, 2011. 3501, 3508

Filippi, J.-B., Bosseur, F., Mari, C., Lac, C., Moigne, P. L., Cuenot, B., Veynante, D., Cariolle, D., and Balbi, J.-H.: Coupled atmosphere-wildland fire modelling, Journal of Advances in Modeling Earth Systems 1, 1–9, 2009. 3502

Filippi, J.-B., Bosseur, F., Pialat, X., Santoni, P.-A., Strada, S., and Mari, C.: Simulation of coupled fire/atmosphere interaction with the MesoNH-ForeFire models, Journal of Combustion, 2011, 540390, doi:10.1155/2011/540390, 2011. 3502

NHESSD
2, 3499–3531, 2014

Finney, M.: FARSITE: Fire Area Simulator – model development and evaluation, Report, US Department of Agriculture, Forest Service, Rocky Mountain Research Station, Fort Collins, CO, 1998. 3517
Forthofer, J. and Goodrick, S.: Review of vortices in wildland fire, Journal of Combustion, 2011, 984363, doi:10.1155/2011/984363, 2011. 3516
Justus, C., Hargraves, W., and Yalcin, A.: Nationwide assessment of potential output from wind-powered generators, J. Appl. Meteorol., 15, 673–678, 1976. 3507
Kirkil, G., Mirocha, J., Bou-Zeid, E., Chow, F., and Kosovic, B.: Implementation and evaluation of dynamic subfilter-scale stress models for large-eddy simulation using WRF, Mon. Weather Rev., 140, 266–284, 2012. 3503
Klemp, J., Dudhia, J., and Hassiotis, A.: An upper gravity-wave absorbing layer for NWP applications, Mon. Weather Rev., 136, 3987–4004, 2008. 3505
Kochanski, A. K., Beezley, J. D., Mandel, J., and Clements, C. B.: Air pollution forecasting by coupled atmosphere-fire model WRF and SFIRE with WRF-Chem, in: 4th Fire Behaviour and Fuels Conference, 2013a. 3503
Kochanski, A. K., Jenkins, M., Krueger, S. K., Mandel, J., and Beezley, J. D.: Real time simulation of 2007 Santa Ana fires, Forest Ecol. Manag., 15, 136–149, 2013b. 3503
Kochanski, A. K., Jenkins, M. A., Mandel, J., Beezley, J. D., Clements, C. B., and Krueger, S. K.: Evaluation of WRF-SFIRE performance with field observations from the FireFlux experiment, Geosci. Model Dev., 6, 1109–1126, doi:10.5194/gmd-6-1109-2013, 2013c. 3503
Kochanski, A. K., Jenkins, M. A., Sun, R., Krueger, S., Abedi, S., and Charney, J.: The importance of low-level environmental vertical wind shear to wildfire propagation: proof of concept, J. Geophys. Res. Atmos., 118, 8238–8252, 2013d. 3503
Lafore, J. P., Stein, J., Asencio, N., Bougeault, P., Ducrocq, V., Duron, J., Fischer, C., Héreil, P., Mascart, P., Masson, V., Pinty, J. P., Redelsperger, J. L., Richard, E., and Vilà-Guerau de Arellano, J.: The Meso-NH Atmospheric Simulation System. Part I: adiabatic formulation and control simulations, Ann. Geophys., 16, 90–109, doi:10.1007/s00585-997-0090-6, 1998. 3502
Linn, R., Reisner, J., Colman, J., and Winterkamp, J.: Studying wildfire behaviour using FIRETEC, Int. J. Wildland Fire, 11, 233–246, 2002. 3502
Linn, R., Winterkamp, J., Edminster, C., Colman, J., and Smith, W.: Coupled influences of topography and wind on wildland fire behaviour, Int. J. Wildland Fire, 16, 183–195, 2007. 3502

NHESSD
2, 3499–3531, 2014

Mandel, J., Beezley, J. D., and Kochanski, A. K.: Coupled atmosphere-wildland fire modeling with WRF 3.3 and SFIRE 2011, Geosci. Model Dev., 4, 591–610, doi:10.5194/gmd-4-591-2011, 2011. 3501, 3503, 3504, 3509

McRae, R.: Breath of the dragon – observations of the January 2003 ACT Bushfires, in: Bushfire Conference 2004: Earth, Wind and Fire – Fusing the Elements, South Australian Department of Environment and Heritage, 2004. 3501

Mirocha, J., Lundquist, J., and Kosovic, B.: Implementation of a nonlinear subfilter turbulence stress model for large-eddy simulation in the Advanced Research WRF model, Mon. Weather Rev., 138, 4212–4228, 2010. 3503

Moeng, C., Dudhia, J., Klemp, J., and Sullivan, P.: Examining two-way grid nesting for large eddy simulation of the PBL using the WRF model, Mon. Weather Rev., 135, 2295–2311, 2007. 3503

Peace, M. and Mills, G.: A case study of the 2007 Kangaroo Island bushfires, Report, Bureau of Meteorology, Australia, 2012. 3503

Pimont, F., Dupuy, J.-L., and Linn, R.: Coupled slope and wind effects on fire spread with influences of fire size: a numerical study using FIRETEC, Int. J. Wildland Fire, 21, 828–842, 2012. 3502

Price, O. and Sharples, J.: The effects of fire channelling on fire severity in the 2009 Victorian fires, Australia, in: 20th International Congress on Modelling and Simulation, edited by Piantadosi, J., Anderssen, R., and Boland, J., available at: http://www.massanz.org.au/modsim2013/A3/price.pdf, 2013. 3501

Rothermel, R.: A mathematical model for predicting fire spread in wildland fuels, Report, Intermountain Forest and Range Experiment Station, Forest Service, US Department of Agriculture, 1972. 3504, 3517

Sharples, J., Viegas, D., Rossa, C., and McRae, R.: Small-scale observations of atypical fire spread caused by the interaction of wind, terrain and fire, in: VI International Conference on Forest Fire Research, edited by: Viegas, D., 2010. 3501, 3508

Sharples, J., McRae, R., and Wilkes, S.: Wind-terrain effects on the propagation of large wildfires in rugged terrain: fire channelling, Int. J. Wildland Fire, 21, 599–614, 2012. 3501, 3511, 3514, 3516, 3517

Sharples, J., Simpson, C., and Evans, J.: Examination of wind speed thresholds for vorticity-driven lateral fire spread, in: 20th International Congress of Modelling and Simulation, edited by: Piantadosi, J., Anderssen, R., and Boland, J., available at: http://www.mssanz.org.au/

NHESSD
2, 3499–3531, 2014

modsim2013/A3/sharples3.pdf, 2013a. 3501, 3502, 3503, 3506, 3507, 3510, 3514, 3515, 3516

Sharples, J., Towers, I., Wheeler, G., Wheeler, V.-M., and McCoy, J.: Modelling fire line merging using plane curvature flow, in: 20th International Congress on Modelling and Simulation, edited by: Piantadosi, J., Anderssen, R., and Boland, J., available at: http://www.mssanz.org.au/modsim2013/A3/sharples2.pdf, 2013b. 3501

Simpson, C., Sharples, J., Evans, J., and McCabe, M.: Large eddy simulation of atypical wildland fire spread on leeward slopes, Int. J. Wildland Fire, 22, 282–296, 2013. 3501, 3502, 3503, 3506, 3507, 3510, 3514, 3515

Skamarock, W., Klemp, J., Dudhia, J., Gill, D., Barker, D., Duda, M., Huang, X.-Y., Wang, W., and Powers, J.: A description of the Advanced Research WRF Version 3, Report, NCAR, available at: http://www.mmm.ucar.edu/wrf/users/docs/, 2008. 3503

Sullivan, A.: Wildland surface fire spread modelling, 1990–2007, 1: physical and quasi-physical models, Int. J. Wildland Fire, 18, 349–368, 2009a. 3501

Sullivan, A.: Wildland surface fire spread modelling, 1990–2007, 2: empirical and quasi-empirical models, Int. J. Wildland Fire, 18, 369–386, 2009b. 3501

Sullivan, A.: Wildland surface fire spread modelling, 1990–2007, 3: simulation and mathematical analogue models, Int. J. Wildland Fire, 18, 387–403, 2009c. 3501

Viegas, D.: A mathematical model for forest fires blow-up, Combust. Sci. Technol., 177, 27–51, 2005. 3501

Viegas, D., Raposo, J., Davim, D., and Rossa, C.: Study of the jump fire produced by the interaction of two oblique fire fronts, Part I: analytical model and validation with no-slope laboratory experiments, Int. J. Wildland Fire, 21, 843–856, 2012. 3501

NHESSD

2, 3499–3531, 2014

Table 1. Time after ignition and lowest height on leeward slope at which the initial lateral spread occurs for each coupled simulation. Also included is the time after ignition at which the fire perimeter first reaches the ridge line.

Simulation	Northerly lateral spread		Southerly lateral spread		Ridge
	Height (m)	Time (min)	Height (m)	Time (min)	(min)
C25	300	10	280	9	17
C30	300	9	300	7	16
C40	300	17	400	23	24
C50	380	26	500	33	33
C60	380	29	480	38	40
C70	440	29	280	20	44
C80	420	37	N/A	N/A	70
C90	380	32	N/A	N/A	75

NHESSD
2, 3499–3531, 2014

Fig. 1. Variation in time of the combined sensible and latent (i.e. total) heat flux for an SFIRE model grid cell immediately following its ignition in WRF-Fire. The calculated values will differ slightly from the actual fuel model values due to the use of 1 min interval WRF-Fire model output.

NHESSD
2, 3499–3531, 2014

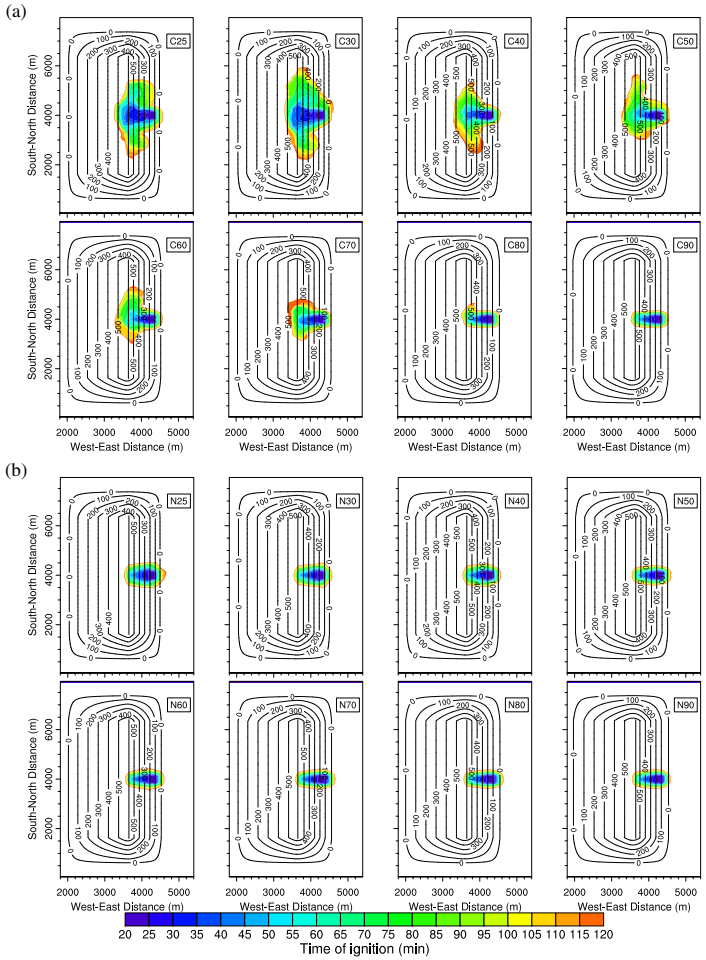

Fig. 2. Time of ignition (min) for each SFIRE model grid cell and terrain height (m) line contours for each **(a)** coupled and **(b)** non-coupled simulation. Simulation names are provided in the top-right corner of each individual plot.

NHESSD
2, 3499–3531, 2014

Resolving vorticity-driven lateral fire spread

C. C. Simpson et al.

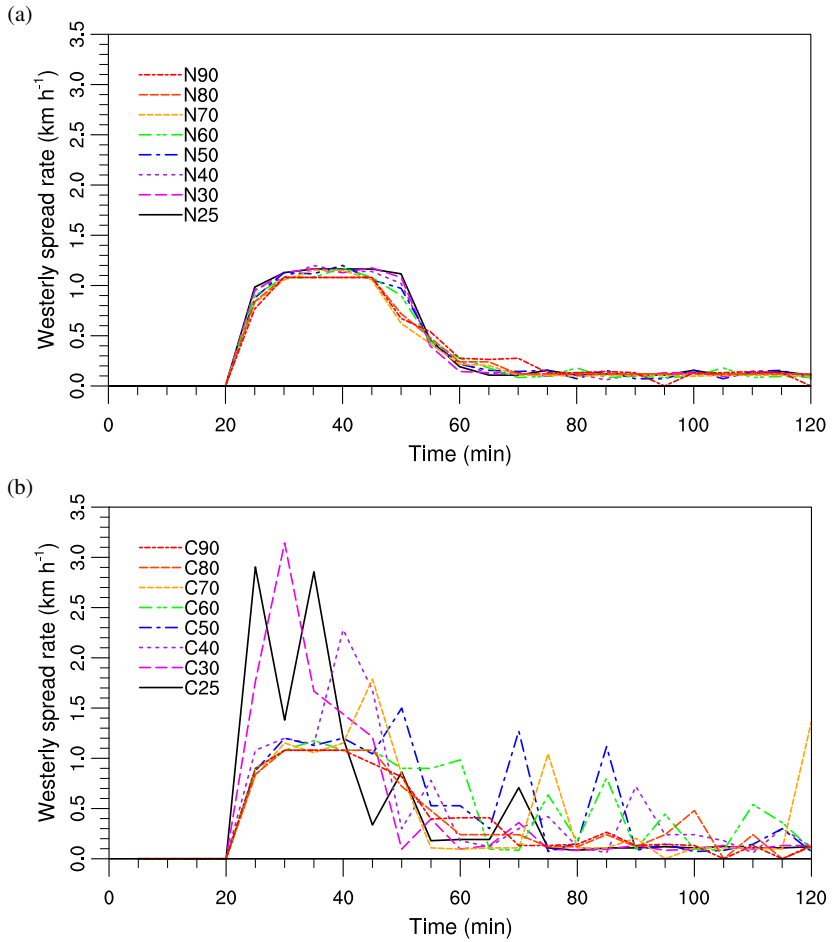

Fig. 3. Westerly spread rate ($km\,h^{-1}$), based on 5 min averaging, following the prescribed ignition for each **(a)** non-coupled and **(b)** coupled simulation.

NHESSD
2, 3499–3531, 2014

Resolving vorticity-driven lateral fire spread

C. C. Simpson et al.

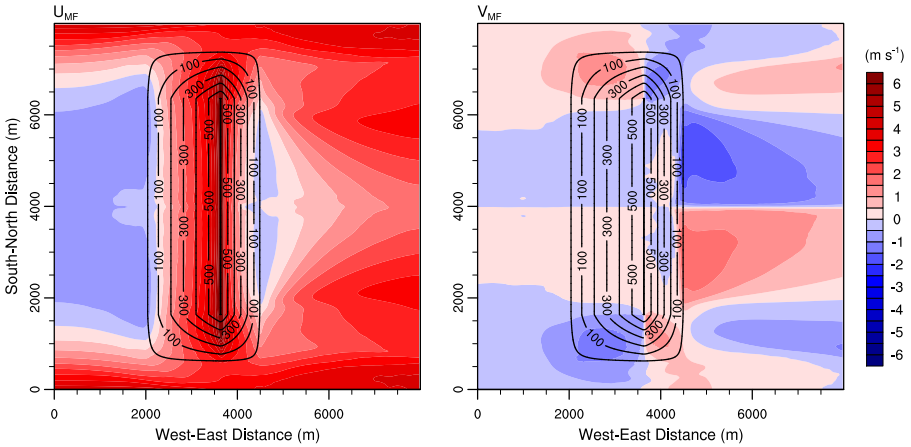

Fig. 4. Average mid-flame height **(a)** *U* and **(b)** *V* component wind speed (m s^{-1}), based on time averaging from 20 to 120 min, for the N25 simulation.

NHESSD
2, 3499–3531, 2014

Resolving vorticity-driven lateral fire spread

C. C. Simpson et al.

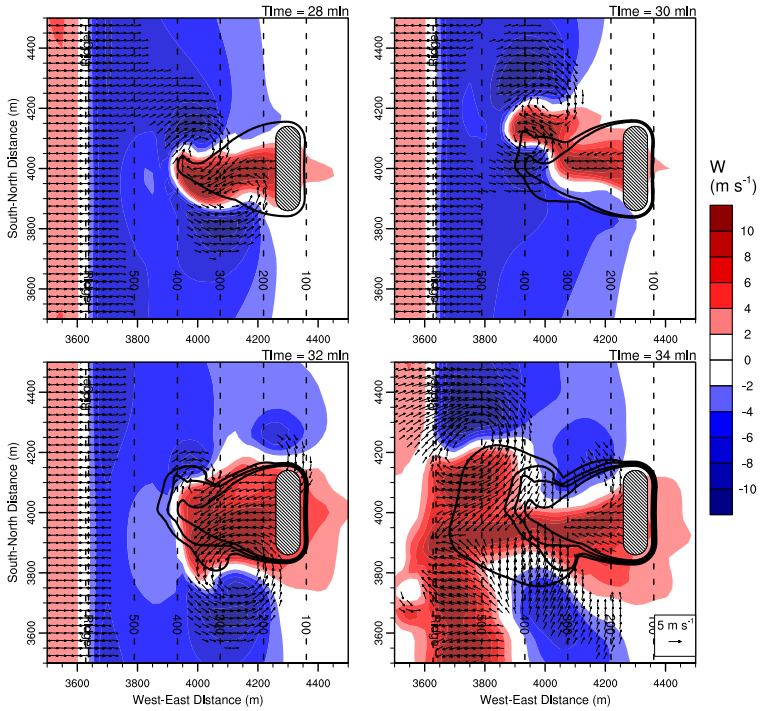

Fig. 5. Vertical velocity, W ($m\,s^{-1}$), at approximately 40 m a.g.l. and horizontal mid-flame height wind vectors, where the wind speed is at least $5\,m\,s^{-1}$, at a time of **(a)** 28 **(b)** 30 **(c)** 32 and **(d)** 34 min for the C25 simulation. The expanding fire perimeter every 2 min is shown by the thick black lines, whereas the dashed lines indicate the terrain height at 100 m intervals. A reference westerly wind vector of $5\,m\,s^{-1}$ is shown in the bottom right of **(d)**, and the dashed pattern filled region indicates the prescribed ignition region.

NHESSD
2, 3499–3531, 2014

Resolving vorticity-driven lateral fire spread

C. C. Simpson et al.

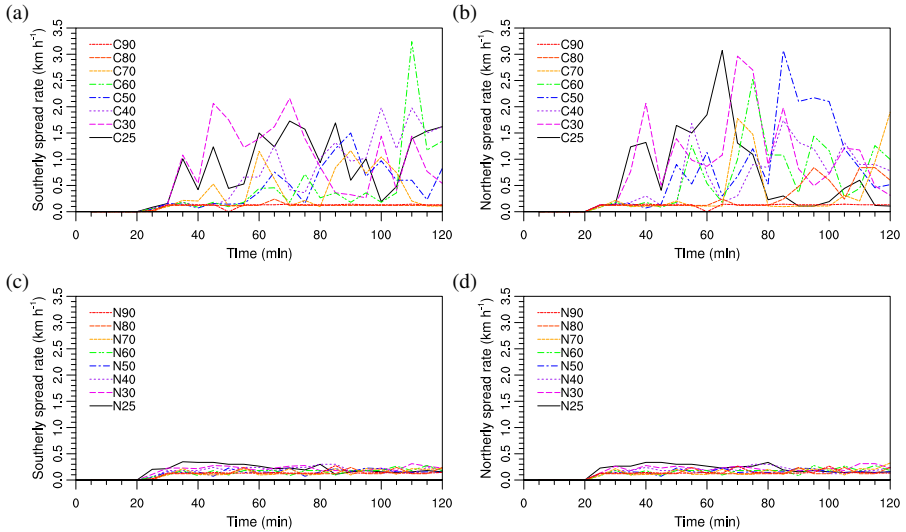

Fig. 6. Southerly and northerly spread rate ($km\,h^{-1}$), based on 5 min averaging, following the prescribed ignition for each **(a, b)** coupled and **(c, d)** non-coupled simulation.

NHESSD
2, 3499–3531, 2014

Resolving vorticity-driven lateral fire spread

C. C. Simpson et al.

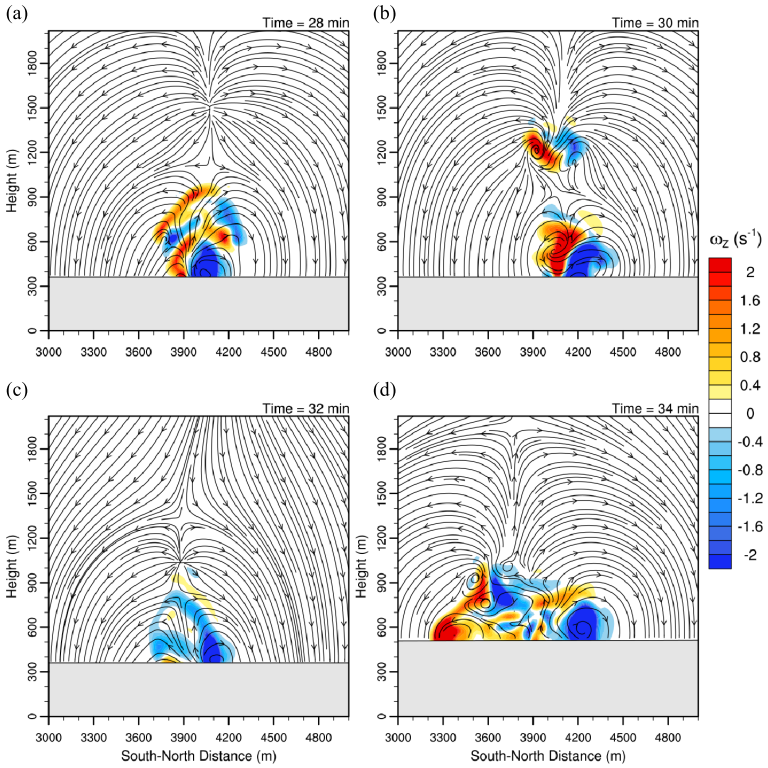

Fig. 7. Magnitude of the vorticity along the $\hat{\mathbf{z}}$ unit vector direction, ω_Z (s^{-1}), and streamlines derived from the *V* and *W* component winds along a vertical cross-section parallel to the ridge line, and through the leeward slope, at a time of **(a)** 28 **(b)** 30 **(c)** 32 and **(d)** 34 min for the C25 simulation. The cross-sections are taken at a west-east distance of **(a, b, c)** 4000 and **(d)** 3800 m, and the grey-filled region indicates the height of the leeward slope along the cross-section.

NHESSD
2, 3499–3531, 2014

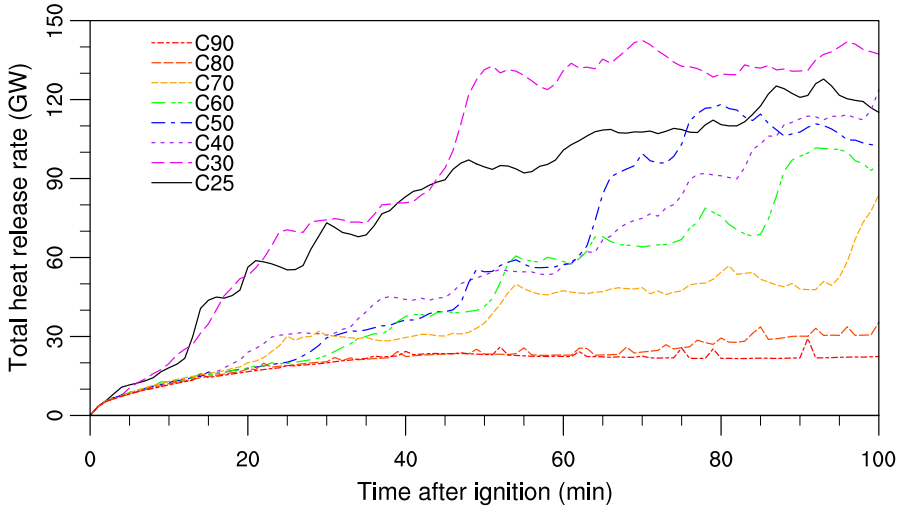

Fig. 8. Variation in time of the domain-aggregated combined sensible and latent (i.e. total) heat release rate (GW) for each coupled simulation.

NHESSD
2, 3499–3531, 2014

Resolving vorticity-driven lateral fire spread

C. C. Simpson et al.

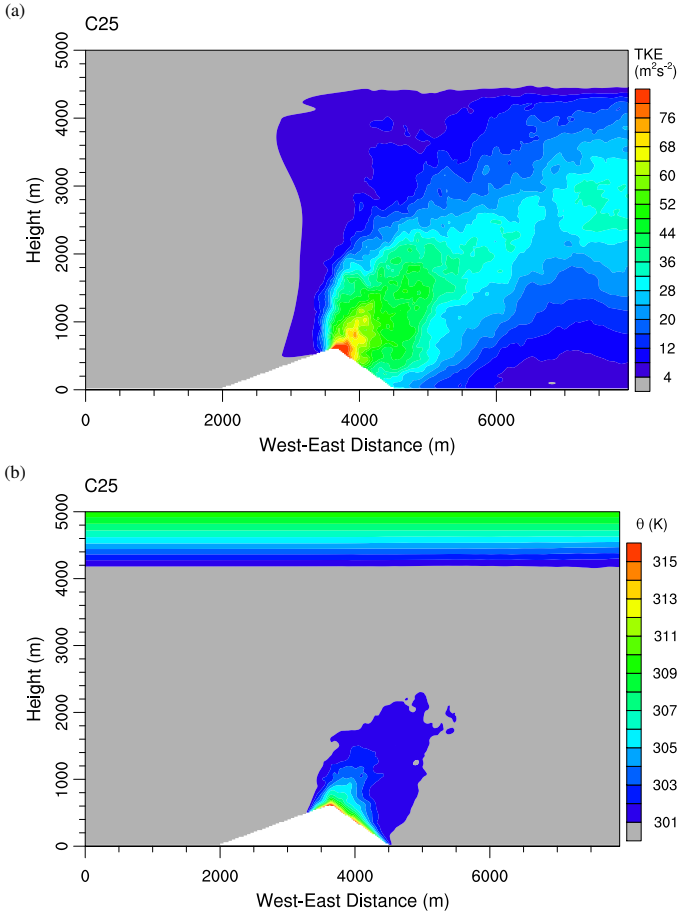

Fig. 9. (a) Resolved turbulent kinetic energy ($m^2 s^{-2}$) and **(b)** potential temperature, averaged from 20 to 120 min, along a vertical cross-section through the centre of the WRF-Fire model domain for the C25 simulation.

NHESSD
2, 3499–3531, 2014